

Fluorinated zirconia-based sol-gel hybrid coatings on polycarbonate with high durability and improved scratch resistance

Raffaella Suriano *, Riccardo Ciapponi, Gianmarco Griffini, Marinella Levi, Stefano Turri

Department of Chemistry, Materials and Chemical Engineering "Giulio Natta", Politecnico di Milano, Piazza Leonardo da Vinci 32, 20133 Milano, Italy.

Hard, scratch-resistant and transparent fluoropolymer-based hybrid coatings are successfully prepared through the sol-gel chemistry and investigated, in the attempt to correlate the chemical, physical and surface properties of these materials with the mechanical properties (i.e. hardness and elastic modulus) measured at the nanoscale by atomic force microscopy (AFM). The organic component of these coatings consists in a hydroxyl-functional fluoropolymer resin, which belongs to the class of chlorotrifluoroethylene-vinylether copolymers and exhibits remarkable properties such as easy handling, great weather resistance, good adhesion and flexibility of coatings. A functionalization of this copolymer is also performed using an isocyanate-functionalized silane in order to assure a covalent cross-linking of organic fluorinated resin with inorganic phases. The combination of the silanized chlorotrifluoroethylene-vinylether copolymer with different sols composed of silica and zirconia is used to obtain high scratch resistance and high durability coatings on polycarbonate. A series of three hybrid coatings with different zirconia/silica molar ratios (0.09/0.48) are developed and analyzed by differential scanning calorimetry (DSC), water contact angle measurements, pencil hardness and adhesion tests. AFM scratch hardness, coating wettability and surface composition measured by Fourier transform infrared spectroscopy (FTIR) are regularly monitored over long-term UV-vis light exposure, to assess the durability of the hybrid coatings. Interestingly, the hybrid fluorinated coatings exhibit an improved scratch resistance and a superior long-term stability when exposed to an accelerated weathering, compared to pristine PC substrates. The mixed silica/zirconia hybrid coatings with a low and intermediate zirconia-to-silica ratio also show excellent mechanical strength, high level of hardness and superior integrity after long-term light exposure.

Keywords: Sol-gel hybrid coating, Hardness, Durability, AFM indentation, Nanoscratch, Adhesion

1. Introduction

Transparent engineering plastics such as polycarbonate (PC) are recognized as the material-of-choice in an ever-increasing range of applications from photovoltaic devices [1–2] to display panels as well as optical lenses [3], compact disks, safety windows and automotive glazing [4–5]. PC particularly offers the advantage of reducing manufacturing costs and product weight when compared to other inorganic transparent materials such as glass. Despite its good optical properties and high resistance to impact and fracture, PC exhibits some weaknesses, such as poor resistance to scratching and UV exposure. To increase the durability and the surface performances of the final product, transparent hard coatings incorporating UV-absorbing molecules are often used as a solution to counteract these problems [6–8].

Silica-based coatings have usually been investigated and applied onto PC by means of various methods, e.g. physical vapor deposition,

plasma enhanced chemical vapor deposition [9] and atmospheric plasma deposition [10]. However, these deposition approaches require expensive instrumentation in order to be implemented and often show a lack of versatility in terms of size and shape of substrates that can be chosen. In addition to those technologies, sol-gel process has been extensively explored, enabling the significant improvement of PC mechanical performances with the added advantage of low capital costs and easy procedures of implementation [11].

The sol-gel process is a well-known method, initially developed to prepare inorganic materials such as glass and ceramics [12]. Typically starting from a metalloid alkoxide precursor $M(OR)_n$ in a liquid medium, the sol-gel process generates an inorganic network through hydrolysis and condensation reactions [13]. By incorporating polymeric or oligomeric organic species into the inorganic network, organic/inorganic hybrid materials can also be produced by means of sol-gel processes. The introduction of the organic components has the advantage of enhancing flexibility, reducing brittleness of the final material and increasing the adhesion to polymer substrates, while keeping high level of hardness and stiffness generally provided by the inorganic phase [14].

Article history:

Received 12 September 2016

Revised 22 December 2016

Accepted in revised form 23 December 2016

Available online 26 December 2016

* Corresponding author.

E-mail address: raffaella.suriano@polimi.it (R. Suriano).

A great variety of inorganic and organic precursors are available and the bulk and surface properties of the resulting coatings can be tailored by selecting the suitable starting reagents [15–17].

Regarding the inorganic phase, silica alkoxides are usually employed as precursors of inorganic networks, but also metal alkoxides (such as those of aluminum, titanium and zirconium) are frequently used, due to the possibility to obtain hybrid coatings with improved mechanical and optical properties [18–19]. Particularly, zirconia-based hybrid coatings are well-known for their excellent mechanical strength, thermal durability as well as anticorrosion properties compared to other ceramic materials [20–22]. A major hitch of the sol-gel process for the preparation of these multicomponent oxide systems is however the different hydrolysis and condensation rates of the precursors, which can lead to heterogeneous mixtures. In order to control the hydrolysis and condensation kinetics of metallic precursors such as zirconium alkoxides that usually react faster than silica ones, chelating agents of metallic centers i.e. acetic acid, acetylacetone and methacrylic acid are frequently necessary and added [22–23].

To obtain a good interpenetration of organic and inorganic phases, covalent bonding between organic components and inorganic networks is preferred. In light of this, three main approaches have so far been adopted in the choice of organic components: (i) the use of low molecular weight organoalkoxysilanes, such as octyltriethoxysilane or triethoxyphenylsilane that introduce small organic domains within the inorganic network; (ii) the incorporation of a curable organoalkoxysilane $R'Si(OR_3)_2$ where the R' is a polymerizable group, e.g. 3-(trimethoxysilyl)propylmethacrylate [24] and 3-glycidoxypropyltrimethoxysilane; (iii) the addition of an organic resin (e.g. acrylate or polyurethane resins) [11]. Among these approaches, the use of fluoropolymer resins and fluorinated organically modified silicates has gained attention in the last few years since these types of materials exhibited important properties for a wide variety of applications, including antimicrobial devices [25], self-cleaning superhydrophobic coatings [26], antifouling coatings for heat exchangers and stainless steel components [27–28] as well as nanocomposites for solar cells and optical devices [29].

Here, we report the simple preparation of a new type of sol-gel hybrid coatings based on a mixed oxide system composed of silica and zirconia with enhanced scratch hardness and elastic modulus for outdoor applications as protective coatings on PC substrates. A chlorotrifluoroethylene-vinylether copolymer with hydroxyl functional groups was selected as the organic component for this work, aiming for excellent outdoor durability, good transparency and solvent resistance. High weather resistance can be guaranteed by the fluorinated segments, while vinyl ether comonomers provide the polymer with various properties such as solubility in organic solvents, flexibility and transparency [30]. Moreover, the presence of hydroxyl groups in the fluorinated resin enabled us to functionalize the polymer with an isocyanate alkoxysilane in order to obtain an organic network crosslinked with the inorganic components. Silica hybrid coatings obtained with this functionalized copolymer and a high content of a silica-based sol has already proven to provide the coating with very good mechanical properties [31]. In a previous study by our group, a mixed silica-titania system was also evaluated to investigate the effect of Ti-O-Si and Ti-O-Ti network on the mechanical properties [32]. However, a decrease in the scratch resistance and comparable values of elastic moduli were observed in that mixed oxide system when compared to the single oxide coating with a similar inorganic content.

In contrast to the previous work, sol-gel hybrids containing a mixture of silica and zirconia were formulated in the present study with the aim of improving the durability and performance of the hybrid coatings. The effect of different zirconia-to-silica ratios on the chemical, physical and nano-mechanical properties of the developed materials was investigated in this work on compositions having a constant inorganic-to-organic weight ratio. These sol-gel hybrid materials were successfully applied on PC substrates by spin-casting sols containing a

silanized fluoropolymer and silica and zirconia precursors. By tuning the chemical composition of the sol gel precursors, their reaction kinetics were successfully controlled and transparent coatings could be obtained, thus preventing any sol destabilization. Moreover, the fluorinated hybrid coatings showed good transparency and adhesion to PC surfaces as well as excellent scratch resistance. To the best of our knowledge, this is the first example of zirconia-based fluorinated hybrid coatings on polymer substrates with high mechanical properties and superior outdoor durability. This work provides a novel and straightforward approach for the development of high performance protective coatings that may find direct application in several technological fields including optical elements, touch-screen devices, automotive components and solar cells.

2. Materials and methods

2.1. Materials

Tetraethylorthosilicate (TEOS), zirconium propoxide 70 wt.% in 1-propanol (ZrP), 3-(triethoxysilyl) propyl isocyanate (IPTES), dibutyltin dilaurate (DBTDL), 2-butanone (MEK), 2-propanol (IPA), methanol (MeOH) and ethanol (EtOH) were supplied by Sigma Aldrich. Glacial acetic acid was purchased by J.T. Baker Chemicals. The fluorocarbon resin Lumiflon LF-910 LM is a chlorotrifluoroethylene-vinylether copolymer (CTFE-VE, for brevity) provided by Asahi Glass Company Ltd (Japan) [33]. It was used as a starting fluoropolymer resin for the following functionalization steps described in the next section. All the products were used without any further purification.

2.2. Functionalization of fluorocarbon resin

The CTFE-VE resin was functionalized according to the procedure reported in a previous paper [32] with minor modifications as briefly described in the following. In a 250 mL three-necked round-bottomed flask equipped with a reflux condenser and a nitrogen gas inlet system, 40 g of CTFE-VE were mixed with 3.88 g of IPTES using a ratio of NCO/OH equivalent ratio of 1/3. This ratio was selected based on a preliminary assessment of the stability of the formulation as it was found to guarantee compatibility with the inorganic phase while maintaining an acceptable shelf-life for the functionalized resin FEVEsil. The hydroxyl equivalents in the Lumiflon resin are provided by the supplier and expressed as mass of potassium hydroxide necessary to neutralize 1 g of resin (for brevity, OH number = 100 mg of KOH per gram of resin). It is important to underline that CTFE-VE resin was supplied as a 66 wt.% solution in xylene and therefore the dry polymer content was only considered for stoichiometric calculations. The initial amount of Lumiflon resin added to the flask was 40 g, which thus corresponded to a dry polymer content of 26.4 g. Taking into account that the OH number, i.e. mg of KOH per gram of polymer, was 100, the equivalent moles of OH in the dry CTFE-VE resin were 0.0471 mol and can be calculated as follows:

$$\begin{aligned} \text{eqOH} &= g_{\text{polymer}} \cdot \text{OHnumber} \cdot \frac{1}{\text{MW}_{\text{KOH}}} \\ &= 26.4 \text{ g} \cdot \frac{0.1 \text{ g KOH}}{g_{\text{polymer}}} \cdot \frac{1}{56.1 \frac{\text{g}}{\text{mol}}} = 0.0471 \text{ mol} \end{aligned} \quad (1)$$

The selected NCO/OH equivalent ratio was 1/3 and therefore 0.0157 mol of NCO were added to the fluoropolymer that corresponded to 3.88 g of IPTES.

Then, the reaction was catalyzed by using DBTDL with a concentration of 0.3 wt.% with respect to the polymer mass. The catalyst was added to the flask as a 1 wt.% solution in ethyl acetate (e.g. 7.92 g of this solution containing 79.2 mg of DBTDL). The reaction was carried out in an inert nitrogen atmosphere at 75 °C under constant stirring

for 2 h. To determine the extent of reaction, a drop of the reaction mixture was placed every hour on a polished NaCl IR crystal window until the absorbance peak of NCO groups disappeared in Fourier transform infrared spectroscopy (FTIR) spectra of the reaction mixture. This process was monitored by FTIR using a Jasco FT-IR 615 spectrometer in the 4000–600 cm^{-1} wavenumber range. The final product, named FEVEsil, was diluted with EtOH (FEVEsil concentration = 50 wt.%) to decrease its viscosity and allow easier handling.

2.3. Preparation of the organic–inorganic hybrid sols

The mixed oxide zirconia/silica coatings were prepared by mixing two different solutions, prepared separately due to the different hydrolysis rates of silicon and zirconium alkoxides [34]. The first solution was composed of a mixture of FEVEsil and TEOS, diluted in EtOH. After 1 h of magnetic stirring at room temperature, an aqueous solution of HCl, composed of 0.1 g (0.001 mol) of HCl 37 wt.% and 0.9 g (0.05 mol) of water, was added dropwise to this solution under stirring. The formulation was allowed to stir magnetically for 1 h to enable the hydrolysis of TEOS. The molar ratio between the components in this first solution was TEOS:EtOH:H₂O:HCl = 1:4.5:3.5:0.07. The second solution was prepared by mixing ZrP with CH₃COOH and then adding H₂O dropwise under stirring. The molar ratio between the components in the second solution was ZrP:CH₃COOH:H₂O = 1:5:4. The two sols were then mixed and stirred for 1 h in order to obtain a homogenous solution. The amounts of each reagent used to prepare the initial solutions and weight percentages of the various components in the final mixed solution are shown in Tables S1 and S2 (please refer to the Supporting information, reagents were considered dry in order to carry out the calculations of the percentages).

Sols containing zirconia gave rise to better coatings if deposited within hours after their preparation. Moreover, these films were prone to precipitation of white zirconia with a consequent loss of transparency when deposited with relative humidity values above a 40% threshold. This phenomenon was probably due to the volatility of the chelating acetic acid and to the higher content of hydrated zirconia with high relative humidity, which is very sensitive to the moisture.

The final sol-gel coatings were obtained after sol deposition (spin-coating, 1200 rpm, 40 s) by heating the as deposited wet films. Heat triggers the condensation of the hydrated oxides, which react with themselves and with the functionalized resin. Coatings were deposited on UV stabilized general purpose PC substrates (PALSUN®, Palmar) and cured at 100 °C for 1 h. Such temperature was chosen in order to avoid distortions of the substrate caused by prolonged exposure to higher temperatures.

According to their zirconia/silica molar ratio, the sol-gel coatings were named as Zr followed by a number indicating the zirconia/silica molar ratio multiplied by 100. Table 1 illustrates the theoretical weight percentages of the different components of the coatings in the gel form and the corresponding molar ratio between silica and zirconia (calculations performed assuming a 100% crosslinking degree).

Table 1
Theoretical weight percentages of the different components and molar ratio between zirconia and silica in the sol-gel hybrid coating, assuming a 100% crosslinking degree.

Coating	Lumiflon wt. %	Silica (IPTES) wt. %	Silica (TEOS) wt. %	Zirconia wt. %	Zirconia/silica molar ratio
Zr9	22.6	0.8	64.3	12.3	0.09
Zr23	22.6	0.8	51.9	24.7	0.23
Zr48	22.6	0.8	38.3	38.3	0.48

2.4. Characterization methods

FTIR spectroscopy was performed with a FT/IR-615 instrument (Jasco Inc.). FTIR spectra were taken on KBr round crystal disks. The analysis was performed by spin-casting the sol on the KBr disk at 1200 rpm for 40 s and then curing it at 100 °C for 1 h. Optical contact angle measurements were carried out using an OCA 20 instrument (Dataphysics Co., Germany), equipped with a CCD photo-camera and with a 500 μL Hamilton syringe to dispense droplets of testing liquids (water, diiodomethane and hexane). Measurements were performed at room temperature, using the sessile drop technique. Using the measured contact angles for the three different wetting liquids, the surface energy for the coatings was derived using the OWRK (Owens, Wendt, Rabel, and Kaible) method, which yields the surface energy of the solid surface with its polar and dispersive components. A DSC 823e (Mettler-Toledo) instrument was used for differential scanning calorimetry (DSC). The analysis consisted of three runs: from 25 °C to 200 °C at 20 °C/min, from 200 °C to 0 °C at –20 °C/min, and from 0 °C to 200 °C at 20 °C/min. The values of glass transition temperatures, T_g obtained from the second heating runs were considered for the discussion in order to exclude any effects induced by a previous mechanical or thermal history. Pull-off tests were performed by gluing a metallic dolly with an epoxy resin to the coated samples. After the complete curing, excess resin was removed and the coating was mechanically cut around the dolly to normalize the resistant area. The dollies were then clamped and pulled with an increasing pressure. When the dolly detached the film from the substrate, the pull off pressure was measured. Tests were performed according to ASTM D4541 standard, with a manual self-aligning tester PosiTest AT (Defelsko corporation, Odgensburg NY), using a bicomponent epoxy resin Araldite 2011 (Huntsman) and curing the glue for 24 h at 40 °C. Four dollies per coating were applied. Pencil scratch hardness measurements were performed according to ASTM D 3363-00 standard. Pencil scratch hardness was measured imposing a mechanical load by means of pencil leads with increasing hardness and reported as the hardness of the hardest pencil that did not scratch the surface. All the hybrid coatings were subjected to weathering tests under continuous Xenon light illumination in a weather-o-meter chamber (Solarbox3000e, Cofomegra S.r.l.) equipped with an outdoor filter cutting all wavelengths below 280 nm, according to ISO 11341. Total irradiance was 550 W/m^2 in the 300–800 nm wavelength range, as measured by means of a power meter with thermopile sensor (Ophir) while the UV light component irradiance in the 295–400 nm range was 58 W/m^2 , as measured by means of a UV-photodiode. All values were kept constant, not simulating day and night cycles. The temperature was maintained at 35 °C with a relative humidity of $20 \pm 3\%$.

2.5. Atomic force microscopy (AFM) nanoscratch tests

To investigate surface hardness at the sub-micron scale, AFM nanoscratch tests were performed with an NSCRIPTOR system using a DNISP nanoindentation probe (Bruker AFM Probes, Camarillo, CA, USA), consisting of a diamond tip with 40 nm radius of curvature mounted on a stainless steel cantilever (calibrated spring constant certified by supplier, $k = 171 \text{ N/m}$). Scratch hardness was evaluated by using a lithographic software (InkCAD by Nanoink) to obtain four 12 μm long scratches with a speed of 0.1 $\mu\text{m/s}$ and additional four scratches with 10 $\mu\text{m/s}$ speed. An average normal load of 66 μN was selected and applied in order to avoid excessive penetration into the coatings (the penetration depth was always lower than 10% of the thickness of the pristine samples). These values of the applied force were calculated by calibrating the deflection sensitivity of the DNISP probe, performing six force-distance curves on a sapphire surface cleaned with isopropanol and dried with nitrogen flux. Scratch widths were evaluated by acquiring topographic $20 \times 20 \mu\text{m}^2$ images of scratches in tapping mode with a resolution of 256 at 0.2 Hz and using ACT-SS

probes purchased from AppNano (Santa Clara, CA). Dynamic hardness H_s was calculated with the following equation:

$$H_s = \eta \frac{F}{w^2} \quad (2)$$

where F is the normal force applied to the tip, η is a constant depending on the tip geometry and w is the scratch width. The geometric constant η is equal to 4.786, as calculated with the following formula for the diamond tip used in this work [35], which is a pyramid with an equilateral triangular base:

$$\eta = \frac{4}{\sqrt{3}} \left(1 + \frac{\tan\beta}{\tan\alpha} \right) \quad (3)$$

where α ($\sim 45.5^\circ$) is the angle between the front edge and the axis of the pyramid and β ($\sim 47.5^\circ$) is the angle between the back face and the axis of the pyramid.

The applied normal force F_N was calculated with the following equation:

$$F_N = \frac{k \cdot z_{(t-b)}}{s} \quad (4)$$

where k is the spring constant of the cantilever, $z_{(t-b)}$ is the vertical displacement of the laser position on the photodetector and s is the sensitivity. By knowing the spring elastic constant and calculating s from calibration curves of the nanoindentation probe on a sapphire reference sample, it is possible to align the photodetector and choose a proper $z_{(t-b)}$ to obtain the desired normal force ($F_N = 66 \mu\text{N}$). Scratch width was measured on three different line profiles, far from the start and the end of the scratch, with a sufficient separation between them. Reported hardness values are the average results of four different scratches, whose width was obtained as described above. Nanoscratch tests were performed on the samples before and after the weathering tests described above. The value of the normal force applied on PC pristine substrates was reduced to $35 \mu\text{N}$ to avoid obtaining scratches of excessive width and depth.

2.6. AFM nanoindentation tests

Elastic modulus of the coatings was evaluated by performing force-distance curves and employing the Hertz and Sneddon models to interpolate the contact part of the force-distance curve, because adhesive interactions between our samples and the AFM tips were neglected. According to the Hertz model [36], the following relation occurs for a spherical indenter with radius of curvature R :

$$F = E_{\text{tot}} R^{1/2} \delta^{3/2} \quad (5)$$

where F is the applied force, δ is the indentation depth and E_{tot} is the total modulus, defined as follows, assuming that the tip is considerably stiffer compared to the samples:

$$\frac{1}{E_{\text{tot}}} = \frac{3}{4} \left(\frac{(1-\nu_s^2)}{E_s} \right) \quad (6)$$

where E_s and ν_s are the elastic modulus and the Poisson's ratio of the sample, respectively.

Starting from this model, another model was proposed by Sneddon [37]. This model is suitable for indenters with a conical shape:

$$F = \frac{2}{\pi} \tan\alpha \frac{E_s}{(1-\nu_s^2)} \delta^2 \quad (7)$$

where α is the half-opening angle of the conical tip. Even if the predominant shape of the tip is a pyramid, the end part is a cone, therefore this

model is suitable for the AFM probes used in this study. The indentation δ is calculated as follows:

$$\delta = (Z_p - Z_{p_0}) - (Z_c - Z_{c_0}) \quad (8)$$

where Z_{p_0} and Z_{c_0} are two values that depend on the chosen model, corresponding to the piezo position and the cantilever deflection in the initial part of the indentation curve, respectively. The equation used to fit the data obtained with a conical tip was the following:

$$k \cdot Z_c = \frac{2}{\pi} \tan\alpha \frac{E_s}{(1-\nu_s^2)} \cdot [(Z_p - Z_{p_0}) - (Z_c - Z_{c_0})]^2 \quad (9)$$

where k , ν_s , α and Z_{c_0} were the parameters whose values is known, while Z_{p_0} and E_s were the parameters whose values were calculated by the interpolation of the data with the models.

For neat PC, Zr9 and Zr23 samples, force distance curves were measured with ACT silicon probes, purchased by AppNano, Santa Clara, CA, with a nominal elastic spring constant $k = 37 \text{ N/m}$, a tip radius $R = 6 \text{ nm}$ and a half-opening angle $\alpha \sim 24^\circ$, according to SEM images [38]. For ACT silicon probes, the actual values of spring constants were calculated with the Sader method [39–40]. The sensitivity value of ACT probes was determined by measuring force distance curves on silicon wafer substrates, previously cleaned by immersion for 30 min in piranha solution (1:3 mixture of H_2O_2 30 wt.% and concentrated sulfuric acid), then rinsing with demineralized water, MeOH and blowing dry with nitrogen. Silicon substrates were also cleaned ultrasonically in EtOH for 15 min and dried with a nitrogen flux. Due to the higher stiffness of the Zr48 coating, the DNISP nanoindentation probe (Bruker AFM Probes, Camarillo, CA, USA) was used to measure force-distance curves on this hybrid coating. The calibrated value of the spring constant for the nanoindentation probe was provided by the supplier ($k = 171 \text{ N/m}$) together with the value of the diamond tip radius ($R = 40 \text{ nm}$). The sensitivity value was calculated by performing force distance curves on a sapphire reference substrate, cleaned with IPA. Instrument parameters were adjusted in order to obtain indentation forces comparable to those used on the other coating systems. The diamond tip has a trapezoidal shape but the indentation depth is comparable to the tip radius. Consequently, the indenter shape can be approximated by a sphere with a radius equal to the radius of the tip. The Hertz model was therefore used to interpolate the experimental points. A Poisson ratio ν_s of 0.2 was used for the hybrid sol-gel coatings [41].

In all cases, the forward and reverse parts of the force-distance curves appeared to be not completely overlapped, especially for PC surfaces. This was caused by the viscoelastic nature of the samples. In order to minimize any non-linear behavior in the determination of the elastic modulus, only the reverse curves were considered for the interpolations with the Sneddon and Hertz models. All the force distance curves were performed at 0.05 Hz.

Fitting of the raw AFM curves was carried out by means of OriginPro 8.5 software and the quality of the fitting was evaluated in terms of coefficient of correlation R^2 (the maximum number of iterations was set to 400 for each fitting). For the fitting, all the datasets were restricted so that the maximum penetration depth of the tip into the sample was not exceeding 0.1% of sample thickness, in order to avoid substrate contributions to the stiffness. The datasets were selected from a statistical point of view according to the method developed in a previous paper [38].

3. Results and discussion

Sol-gel hybrid coatings with a constant amount of fluorinated resin (22.6 wt.%) and increasing zirconia/silica molar ratios (ranging from 0.09 to 0.48) were prepared by spin-coating PC substrates with precursor sol dispersions and subsequently curing the deposited materials at 100°C (Fig. 1, for brevity from here on these coatings will be referred

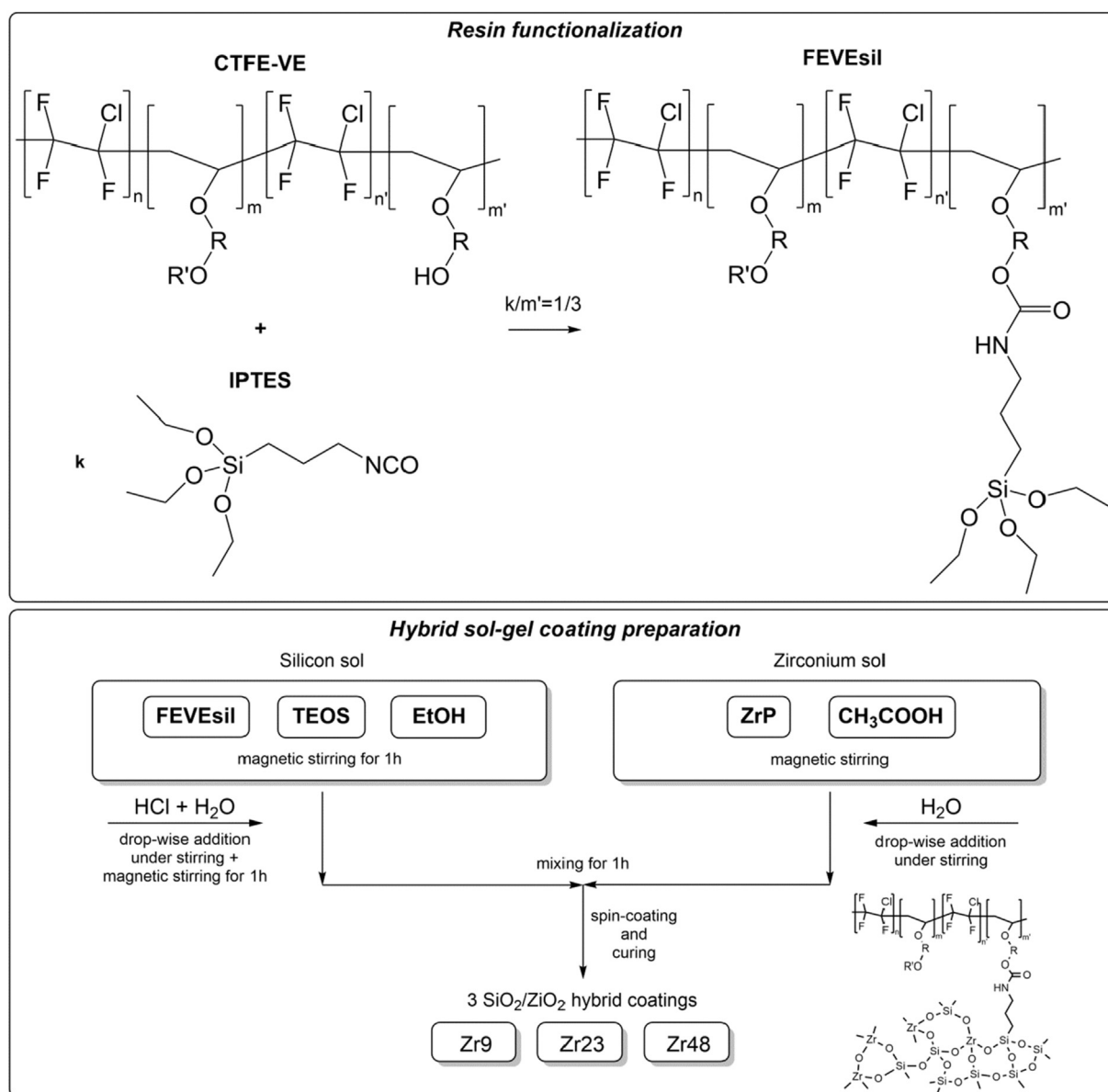


Fig. 1. Schematic representation of the chemical reactions for the functionalization of the fluorinated resin and the preparation of the hybrid sol-gel coatings.

to as Zr followed by a number indicating the molar ratio between zirconia and silica multiplied by 100).

The effect of the amount of zirconia on the physical, chemical and mechanical properties as well as outdoor durability of the newly prepared coatings was thus investigated. All the coatings were obtained as transparent films, indicating the formation of homogenous hybrids without any visible heterogeneous phases (please see the Supporting information, Fig. S1). FTIR spectra of the three hybrid coatings were considered to observe any chemical difference in the inorganic networks

when varying the zirconia/silica molar ratios. As shown by the Fig. S2, the absorbance attributed to Zr—O—Zr bonds and ZrO₂ domains [42] barely appeared only for Zr48 coatings at 644 cm⁻¹ as a shoulder of another peak due to CF₂ wagging. This suggests the presence of ZrO₂ clusters, segregated in nano-domains and dispersed in a silica network, only for zirconia/silica molar ratio higher than 0.5. Consequently, the hybrid systems presented in this work were mainly composed of a homogenous inorganic framework of Zr—O—Si bonds. The glass transition temperature (*T_g*) of the zirconia/silica hybrid coatings was evaluated by

Table 2
Glass transition temperature (*T_g*), pencil hardness on PC surfaces and on glass and PC coated with Zr9, Zr23, and Zr48 coatings and surface energy values calculated according to the OWRK method for PC substrates uncoated and coated with the hybrid sol-gel coatings.

Coating	<i>T_g</i> (°C)	Pencil hardness		Water contact angle (°)	Surface energy (mN/m)		
		On glass	On PC		Dispersive component	Polar component	Total
PC	148.3	n.d.	6B-5B	71 ± 2	36.6 ± 0.9	10.1 ± 0.8	46.6 ± 1.2
Zr9	171.1	2H-3H	B-HB	80 ± 2	26.6 ± 0.8	7.6 ± 0.9	34.2 ± 1.2
Zr23	171.3	2H-3H	B-HB	92 ± 3	28.0 ± 0.7	2.9 ± 0.8	30.9 ± 1.0
Zr48	178.8	3H-4H	B-HB	91 ± 3	26.7 ± 0.9	3.0 ± 1.0	29.7 ± 1.3

means of DSC. For outdoor applications as protective coatings, the T_g of the hybrid materials should be much higher than room temperature in order to minimize degradation effects due to long-term exposure to high temperatures. All the hybrid coatings confirmed to be suitable for outdoor uses because T_g values were found to be much higher than room temperature irrespective of the system (170 °C for Zr9 and Zr23, and 179 °C for Zr48, Table 2).

In order to explore the macroscopic scratch resistance of the coatings, pencil hardness measurements were carried out on all systems (Table 2). All the hybrid coatings deposited on PC exhibited an improved pencil hardness (4 grades higher) when compared to the bare substrate, which was reported to have a 6B grade of pencil hardness [43]. Moreover, the coatings containing both zirconia and silica showed a pencil hardness 1–2 grades higher than that found on single oxide coatings, suggesting a higher macroscopic scratch resistance for mixed oxide coatings. The addition of zirconia therefore proves to be beneficial in terms of coating scratch hardness. When compared to the samples applied on glass, the coatings deposited on PC appeared to be less scratch resistant. These results may be ascribed to the effect of the substrate materials on the macromechanical response of the coatings. Indeed, materials such as PC coated by thin films are known to undergo a plastic deformation and induce a gouge failure on the coating surface, even though the coating shows a high level of hardness [43]. In order to enhance the macroscopic scratch resistance, a higher coating thickness may be employed, as this was proven to prevent the deformation of soft substrates [43].

Static contact angles with water, diiodomethane (DIM) and hexadecane for the different coatings were measured on PC substrates and coatings deposited on PC. The water contact angle values for Zr23 and Zr48 coatings were higher than those measured on other coatings. Indeed, zirconia is less hydrophilic when compared to silica [44], therefore the progressive substitution of the latter with the former results in increased water contact angles for Zr23 and Zr48 coatings. Based on the measured contact angles for water, DIM and hexadecane, the surface energy values for the coatings were calculated by using the OWRK method (Table 2). The surface analysis of the coatings performed with optical contact angle measurements showed that values of the coatings containing zirconia were relatively low. In particular, the polar components, γ_p of the surface energy for the coatings were found to be lower, even with a 70% reduction for Zr23 and Zr48 systems when compared to that observed for PC. This may lead to a reduction of PC degradation under high levels of humidity when coated with Zr23 and Zr48 coatings, thus increasing the hydrolytic stability of the substrate.

In order to evaluate elastic modulus of the hybrid coatings, AFM indentation tests were carried out. The ability of this technique to apply low-magnitude forces results in sufficiently low penetration depths, that enable the study of mechanical properties of thin coatings without any bias induced by the substrates. Table 3 lists: elastic modulus (E) measured for the coatings; max indentation depth (δ) as obtained from the force-distance curves; cantilever spring constant of the probe used as indenter (k); and the corresponding thickness of the coatings (s).

The values of elastic modulus were determined by employing conical silicon tips as indenters and the Sneddon model [37] for the

interpolation of the reverse curves of all samples, except for the high zirconia coatings. Indeed, due to its higher level of stiffness, Zr48 coatings were indented by a diamond tip mounted on a cantilever of higher stiffness. Accordingly, to take into account the different shape and dimensions of the diamond tip used in this case, a different model (i.e. the Hertz model) suitable for spherical tips was employed to interpolate reverse force curves. Elastic modulus for PC substrates was also evaluated by means of AFM indentations. The elastic moduli measured for the hybrid coatings were found to be one order of magnitude higher than PC (Table 3). Taking into account some sources of uncertainty known in AFM-based measurements of material properties such as z-piezo displacement calibration [45], the measured values of elastic modulus obtained for the hybrid coatings newly-presented in this work were found to be comparable to similar fully inorganic samples such as a thin film of SiO₂ ($E = 19$ GPa) [46]. Moreover, Zr9 exhibited an average elastic modulus of 15 GPa, which is very similar to the average value of modulus (16.4 GPa) determined for fluoropolymer-based hybrid coatings with a comparable inorganic-to-organic weight ratio and composed of only silica and fluorinated resin [32]. The elastic modulus for the sol-gel coatings containing zirconia also increased by increasing the amount of zirconia that was incorporated. The progressive addition of zirconia and the mixed oxide network therefore enabled an increase in the elastic modulus. Morphological analysis carried out by AFM imaging on the hybrid coatings also showed the formation of smooth surfaces without any phase separation for Zr23 and Zr48 systems (Supporting information, Table S3, Figs. S3 and S4). As for Zr9, this coating showed higher values of roughness due to the presence of pinholes and cracks at the nanoscale (Figs. S5 and S6). Such pinholes and cracks were likely created due to the faster reactivity of the zirconium hydroxide [42], compared to silicon hydroxide in the sol, which acts as a starting point for the crosslinking reaction. This caused a local increase of by-product evaporation, which produced these holes. Higher values of roughness measured for Zr9 can also explain the higher advancing contact angles observed for these coatings as compared to PC substrates and the other coatings (Table S4).

Pull-off tests were also performed on coatings deposited on PC and glass for the evaluation of the adhesion properties. The hybrid coatings revealed a moderate adhesion on PC surfaces, irrespective of the type and amount of inorganic oxides, as shown in Table 3. These adhesion strength results were found to be in a good agreement with those obtained for a polyurethane coating applied on silane-coated aluminum substrates after drying the specimen [47]. This moderate adhesion is in fact indicative of no covalent bonds between PC chains and the inorganic phase network. When the hybrid coatings were deposited on glass, the glass substrates were broken during pull-off tests without the detachment of the hybrid films from the glass, suggesting that the pull-off strength was higher than the maximum limit of detectable pressure (>8 MPa). These results indicate that the silica network of the coatings can strongly bond to the glass silicon dioxide [48], creating covalent bonds which dramatically increase the adhesion. Nevertheless, the results obtained from pull-off tests were positive, taking into account that no primer layer was applied before the hybrid coating deposition and no physical pre-treatment on the substrates (e.g. plasma treatments) was carried out. In addition, any environmental stress crazing

Table 3

Elastic modulus, maximum indentation obtained from nanoindentation tests, spring constants of the cantilevers used for the tests on pristine PC substrates and PC coated with Zr9, Zr23, and Zr48 coatings, thickness and pull-off strengths measured for the coatings applied on glass and PC substrates.

Coating	Elastic modulus (GPa)	Maximum indentation (nm)	Spring constant (N/m)	Thickness (μ m)	Pull-off pressure (MPa)	
					On glass ^a	On PC
PC	1.0 \pm 0.2	155.4 \pm 20.4	50.8	–		
Zr9	15.1 \pm 4.3	48.0 \pm 10.6	56.1	1.1 \pm 0.1	>8	0.5 \pm 0.1
Zr23	26.6 \pm 5.2	33.5 \pm 6.7	59.3	1.3 \pm 0.1	>8	0.8 \pm 0.3
Zr48	30.9 \pm 3.4	31.0 \pm 5.0	171	1.7 \pm 0.1	>8	0.5 \pm 0.1

^a Cohesive detachment of the substrate.

was not induced on the PC substrates by the solvents used for the sol-gel process and the adhesion strength appeared to not affect the mechanical properties of hybrid coatings, as also observed in a previous paper [6].

Scratch resistance and dynamic hardness were characterized for each of the coatings deposited on PC by performing scratches at the nanoscale by means of AFM nanolithography. The material surface was indented and ploughed by a diamond tip. By applying a normal force constant during the scratch test to the scratching probe, it is possible to calculate the hardness of the indented material by measuring the scratch width, according to the Eq. 2. This allowed us to evaluate the mechanical performance of the coatings without any interference from the substrate. Nanoscratch hardness was measured at different scratching speeds to evaluate possible viscoelastic effects. In addition, we tested the scratch resistance of the coatings over prolonged exposure to UV-vis light (0–1500 h) to assess their outdoor durability. Before the UV-vis light exposure, hardness values in the range of 1–2 GPa were measured for the hybrid coatings. As far as PC is concerned, hardness values of 0.38 ± 0.01 GPa were determined (Fig. 2).

Higher nanoscratch hardness values were determined for Zr23 when compared to the other coatings. Upon UV-vis light exposure, a progressive reduction in hardness values was observed for PC substrates. After 1500 h of accelerated weathering, the values of scratch hardness measured on uncoated PC decreased by 35%. Conversely, the hardness of coatings with a higher content of zirconia appeared to be not affected by the prolonged exposure to UV-light, as also occurred for the Zr23 coatings until 500 h of exposure. After 1500 h in a weather-o-meter chamber, the Zr23 coatings exhibited a 100% increase in the scratch hardness values, reaching a level of hardness of 2.5–3 GPa. A progressive increase in the scratch hardness was also noticed for the hybrid coating with a lower content of zirconia during light exposure. Such improvement in scratch resistance may be due to an environmental post-curing of the coatings. Indeed, when continuously exposed to a temperature of 35 °C, an increase of the cross-linking degree in the sol-gel networks can occur. Moreover, the organic component appeared to be not affected by UV degradation due to its halogenated structure which is particularly resistant to weathering [30]. No significant difference was found in the hardness values of the coatings as observed by performing nanoscratch tests at a higher rate (10 $\mu\text{m/s}$). A different behavior was observed on PC substrates which exhibited a viscoelastic behavior, being stiffer under a faster stimulus (Fig. S7). The high content of inorganic phase in the coatings can account for the comparable values of hardness measured at different rates.

An increase in the crosslinking degree upon weathering experiments was also confirmed by the FTIR spectra of the hybrid coatings that were collected in the effort to explore any changes in the chemical structure of the samples induced by the prolonged light exposure (Fig. 3).

As evidenced by all the spectra collected, a decrease in the OH stretching signals ($3600\text{--}3100\text{ cm}^{-1}$) is observed after 200 h of light exposure. This is likely due to a reduction of hydroxyls in the coatings

ascribable to silicon and zirconium hydroxides that condense into silicon and zirconium oxides by reacting with alkoxides and other hydroxides generating, respectively, alcohol and water as by-products (Fig. S8). After 1000 h of light exposure, another band clearly appears at $1360\text{--}1350\text{ cm}^{-1}$ with a shoulder at $1450\text{--}1400\text{ cm}^{-1}$ that can be respectively related to the symmetric and asymmetric deformation of the aliphatic C—H groups. The increase of this signal can be caused by the photo-oxidative degradation of polymer resin that is initiated by a subtraction of a hydrogen from a methylene in α position to the NH of urethane groups and then followed by the formation of a polymer peroxy radical ($\text{PO}_2\bullet$) and a polymer oxy radical ($\text{PO}\bullet$) [49]. These radicals can respectively produce hydroperoxide (POOH) and hydroxyl (POH) groups but also react with each other leading to crosslinking, resulting in a weak increase of absorption observed in the hydroxyl domain after 1500 h for Zr9 coatings (Fig. S9) and in the presence of CH bending vibration at $1450\text{--}1350\text{ cm}^{-1}$ after 1000 h of light exposure (inset Fig. 3).

Considering the conditions of the weathering tests performed in this work ($T = 35\text{ }^\circ\text{C}$, relative humidity = $20 \pm 3\%$, continuous illumination), the hybrid sol-gel coatings can be considered sufficiently stable to photo-degradation and represent a good solution in the application field of anti-scratch coatings. Conversely, PC substrates appeared to undergo some significant changes after 1500 h of light exposure as evidenced by the new signals emerging between 1750 and 1650 cm^{-1} and at 1430 cm^{-1} , likely due to the formation of carbonyl groups resulting from the photo-oxidative degradation of the polycarbonate (Fig. S10). Indeed, PC undergoes a photo-initiated rearrangement forming phenyl ester groups [50], which possess an infrared absorption at $1740\text{--}1705\text{ cm}^{-1}$. Moreover, the presence of absorption at $1670\text{--}1600\text{ cm}^{-1}$ reveals the occurrence of the so-called photo-Fries rearrangement giving diphenylketone groups [51]. The appearance of weak broad band around $3400\text{--}3100\text{ cm}^{-1}$ also indicates the formation of hydroxyl species and confirms the photo-degradation of PC substrates upon prolonged light exposure.

These results were supported by the measurement of coating wettability over the entire duration of weathering tests. As shown in Fig. 4, where static contact angle measurements with water are presented over prolonged light exposure, water contact angles on PC substrates appeared to slightly increase after 1000 h of light exposure and fell down after 1500 h. This sudden drop after 1500 h was likely due to the formation of oxidized species (highly hydrophilic) in weathered PC surfaces, as also observed by means of FTIR spectroscopy, and to an increase in surface roughness. Indeed, the root-mean-square roughness R_{RMS} of PC after 1500 h ($R_{\text{RMS}} = 56 \pm 13\text{ nm}$) was found to be higher than that measured on non-weathered substrates ($R_{\text{RMS}} = 9 \pm 1\text{ nm}$). As opposed to this, the wettability of the hybrid coatings appeared to be adequately stable upon prolonged light exposure. All the coatings investigated in this work only showed small reductions in water contact angles after 1500 h, probably due to the minor photo-oxidation of the functionalized polymer resin based on urethane groups, previously discussed. A good photo-stability of the hybrid systems newly-developed in this study was also highlighted by the dynamic contact angle

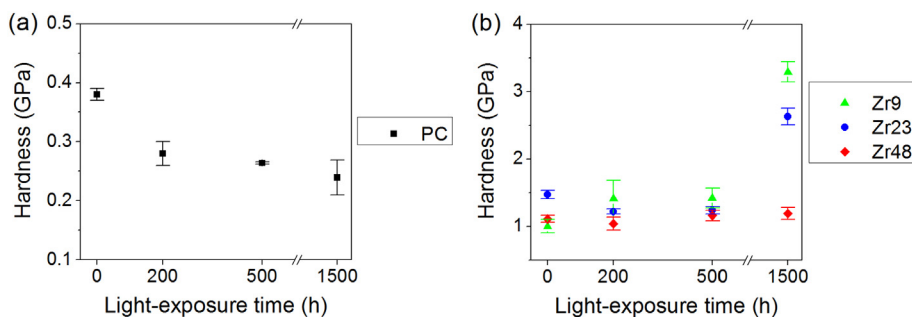


Fig. 2. Nanoscratch hardness over light exposure time of (a) uncoated PC surfaces and (b) coated PC substrates with hybrid sol-gel coatings (Zr9, Zr23, Zr48) measured applying a force of 66 μN at a rate of 0.1 $\mu\text{m/s}$ by means of a diamond tip mounted on the AFM scanner.

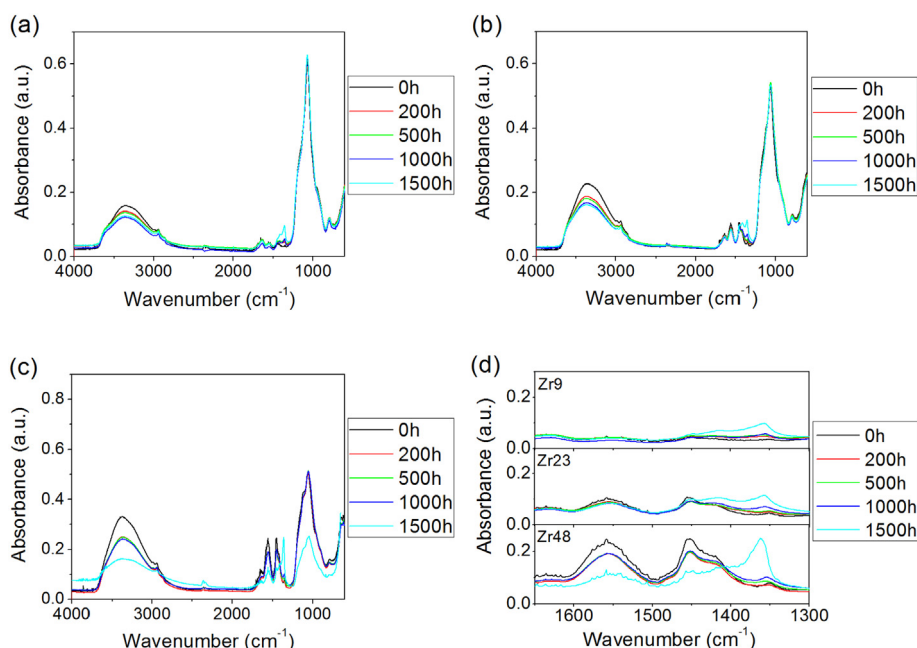


Fig. 3. FTIR absorption spectra of (a) Zr9, (b) Zr23, and (c) Zr48 coatings before (0 h) and after 200 h, 500 h, 1000 h and 1500 h of light-exposure in a weather-o-meter chamber. Spectra were collected and shown in the wavenumber range of 4000–600 cm^{-1} . (d) FTIR absorption spectra of Zr9, Zr23 and Zr48 coatings with the limited wavenumber range of 1650–1300 cm^{-1} .

measurements performed after 1500 h of light exposure time (Table S4). The values of advancing and receding contact angles for all the coatings after weathering tests were found to be only slightly lower than those before light exposure. This result was likely due to the photo-degradation of organic components of the hybrid systems, as already evidenced by static contact angles measurements. On the contrary, dynamic contact angles measured on PC substrates showed a kinetic hysteresis and time-dependent behavior. This can suggest a photo-induced decrease of molecular weights of macromolecules in the outermost layers of PC surfaces that can easily reorient oxidized surface groups in response to changes in the local environment (water drops during dynamic measurements) in order to minimize the free energy at the interface.

The influence of weathering tests was also investigated by observing aged samples under an optical microscope. Fig. 5 presents the optical micrographs of uncoated surfaces and hybrid coatings with different zirconia/silica molar ratio after 1500 h of light exposure. PC surfaces appeared highly rough with some pinholes after 1500 h (Fig. 5a). Zr48 revealed show a pattern of clear cracks, which mostly appeared to be oriented in the same direction (Fig. 5d). An improvement in the morphology was observed on the surface of Zr9 which only showed small and isolated cracks (Fig. 5b). Finally, Zr23 exhibited a flat and smoother

morphology with very few cracks only present in some isolated regions of the coating (Fig. 5c).

4. Conclusions

New silica/zirconia hybrid fluorinated coatings with high scratch resistance and high outdoor durability were successfully developed through the sol-gel chemistry, combining a silanized fluorinated polymer with different sols composed of silica and zirconia. In this study, particular attention was paid to the effect of zirconia-to-silica molar ratio on the physical, chemical and mechanical properties of the hybrid coatings. The sol-gel hybrid materials were applied on PC substrates by spin-coating. Pencil hardness tests confirmed the scratch resistance and durability of the hybrid coatings at the macro-scale. AFM indentation and nanoscratch tests were performed to respectively evaluate the elastic modulus and the dynamic hardness of the hybrid systems, resulting in a high modulus (up to 31 GPa) and high-level scratch hardness (up to 2 GPa). The hybrid coatings were also characterized by FTIR spectroscopy, contact angle measurements and AFM nanoscratch tests during a prolonged exposure to UV-vis light, with the aim of testing outdoor durability and correlating the scratch resistance with possible chemical modifications and wettability behavior. All the coatings exhibited

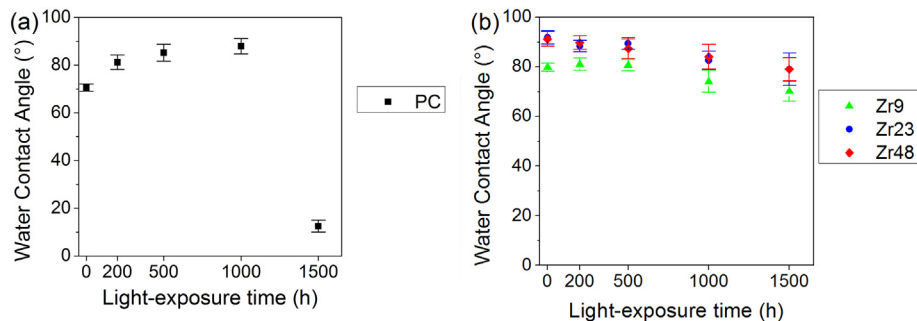


Fig. 4. (a) Water contact angles measured for uncoated substrates (PC) and (b) hybrid sol-gel coatings (Zr9, Zr23, Zr48) before (0 h) and after 200 h, 500 h, 1000 h and 1500 h of light exposure time.

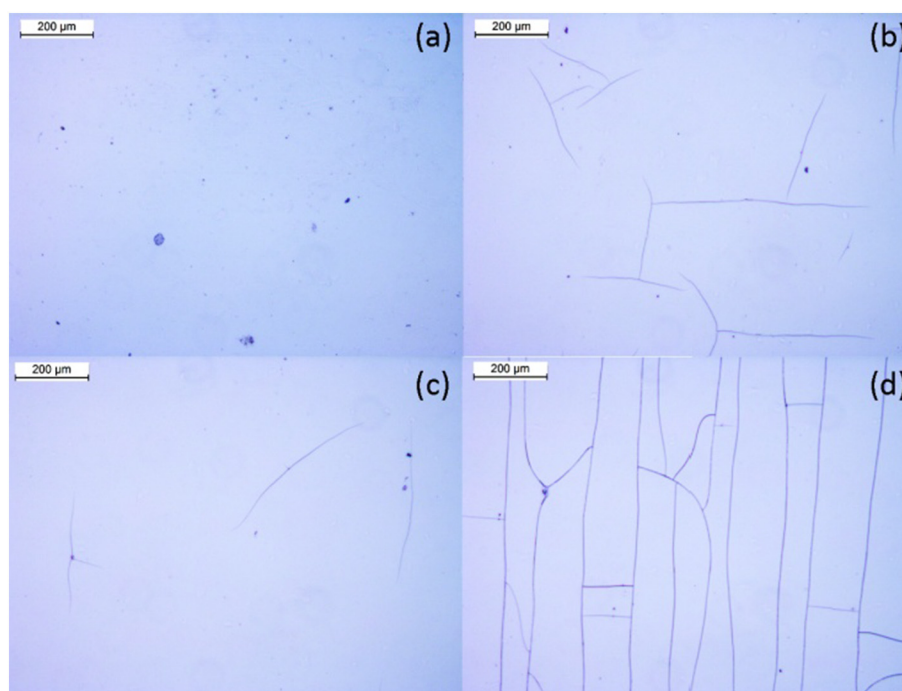


Fig. 5. Optical micrographs for the surfaces of (a) uncoated substrates, (b) Zr9, (c) Zr23, and (d) Zr48 coatings after 1500 h of light exposure in a weather-o-meter chamber.

excellent stability, a moderately good adhesion on PC without the use of any primer or physical treatment and an overall improvement in scratch resistance over long-term light exposure. A different behavior was observed on the coatings with the highest zirconia/silica molar ratio, which revealed no significant changes in scratch hardness. Conversely, the reference PC substrates showed significant photo-degradation and a reduction in scratch hardness by increasing light exposure time. The low and intermediate content of zirconia investigated (zirconia-to-silica molar ratio of 0.09 and 0.23) enabled the hybrid coatings to have a smooth surface morphology even after prolonged light exposure, while maintaining high-level mechanical performance and scratch hardness of nearly 2.5–3 GPa. The results of this study show that silica/zirconia fluorinated hybrids have great potential as hard antiscratch coatings on plastics, providing remarkable durability and mechanical resistance in a straightforward way without requiring complicated steps or expensive instrumentation for their preparation. Additional studies will be carried out in the future to further improve the adhesion of these hybrid systems to plastic substrates, for example, by performing a plasma treatment of substrates before spin-coating. The promising progress evidenced by this study suggests continuing the use of these materials in the field of functional coatings developing their deposition on different substrates such as polymethylmethacrylate (PMMA), polypropylene (PP), polyamides (PA) and acrylonitrile-butadiene-styrene copolymer (ABS). The excellent scratch resistant properties of these hybrid systems would be so exploited with various substrates which find application in a wide number of areas, e.g. automotive field, consumer goods, photovoltaic and optical devices.

Acknowledgements

The authors acknowledge financial support from Progetto Bandiera 'La Fabbrica del Futuro' in the frame of the project 'POLYPHAB—POLYmer nanostructuring by two-Photon ABSorption'.

Appendix A. Supplementary data

Supplementary data to this article can be found online at <http://dx.doi.org/10.1016/j.surfcoat.2016.12.095>.

References

- [1] S.M. El-Bashir, F.M. Barakat, M.S. AlSalhi, Double layered plasmonic thin-film luminescent solar concentrators based on polycarbonate supports, *Renew. Energy* 63 (2014) 642–649.
- [2] D. Azulai, U. Givan, N. Shpaisman, T.L. Belenkova, H. Gilon, F. Patolsky, G. Markovich, On-surface formation of metal nanowire transparent top electrodes on CdSe nano-wire array-based photoconductive devices, *ACS Appl. Mater. Interfaces* 4 (2012) 3157–3162.
- [3] T.W. Boentoro, B. Szyszka, 14 - protective coatings for optical surfaces, in: A. Piegari, F. Flory (Eds.), *Optical Thin Films and Coatings*, Woodhead Publishing 2013, pp. 540–563.
- [4] C. Seubert, K. Nietering, M. Nichols, R. Wykoff, S. Bollin, An overview of the scratch resistance of automotive coatings: exterior clearcoats and polycarbonate hardcoats, *Coatings* 2 (2012) 221–234.
- [5] N. De Vietro, L. Belforte, V.G. Lambertini, F. Fracassi, Low pressure plasma modified polycarbonate: a transparent, low reflective and scratch resistant material for automotive applications, *Appl. Surf. Sci.* 307 (2014) 698–703.
- [6] N. Le Bail, K. Lionti, S. Benayoun, S. Pavan, L. Thompson, C. Gervais, G. Dubois, B. Toury, Scratch-resistant sol-gel coatings on pristine polycarbonate, *New J. Chem.* 39 (2015) 8302–8310.
- [7] C. Präfke, U. Schulz, N. Kaiser, Preparation and characterization of organic layers for UV protection of polycarbonate, *Thin Solid Films* 520 (2012) 4180–4183.
- [8] M. Zayat, P. Garcia-Parejo, D. Levy, Preventing UV-light damage of light sensitive materials using a highly protective UV-absorbing coating, *Chem. Soc. Rev.* 36 (2007) 1270–1281.
- [9] M. Noborisaka, H. Kodama, S. Nagashima, A. Shirakura, T. Horiuchi, T. Suzuki, Synthesis of transparent and hard SiOC(–H) thin films on polycarbonate substrates by PECVD method, *Surf. Coat. Technol.* 206 (2012) 2581–2584.
- [10] L. Cui, A.N. Ranade, M.A. Matos, L.S. Pingree, T.J. Frot, G. Dubois, R.H. Dauskardt, Atmospheric plasma deposited dense silica coatings on plastics, *ACS Appl. Mater. Interfaces* 4 (2012) 6587–6598.
- [11] N. Le Bail, S. Benayoun, B. Toury, Mechanical properties of sol-gel coatings on polycarbonate: a review, *J. Sol-Gel Sci. Technol.* 75 (2015) 710–719.
- [12] J. Wen, G.L. Wilkes, Organic/inorganic hybrid network materials by the sol-gel approach, *Chem. Mater.* 8 (1996) 1667–1681.
- [13] C.J. Brinker, G.W. Scherer, *Sol-gel Science: The Physics and Chemistry of Sol-gel Processing*, Academic Press, Inc., San Diego, 1990.
- [14] K. Lionti, L. Cui, W. Volksen, R. Dauskardt, G. Dubois, B. Toury, Independent control of adhesive and bulk properties of hybrid silica coatings on polycarbonate, *ACS Appl. Mater. Interfaces* 5 (2013) 11276–11280.
- [15] Y. Tokudome, T. Hara, R. Abe, M. Takahashi, Transparent and robust siloxane-based hybrid lamella film as a water vapor barrier coating, *ACS Appl. Mater. Interfaces* 6 (2014) 19355–19359.
- [16] S. Dong, Z. Zhao, R.H. Dauskardt, Dual precursor atmospheric plasma deposition of transparent bilayer protective coatings on plastics, *ACS Appl. Mater. Interfaces* 7 (2015) 17929–17934.
- [17] J.D. Mackenzie, E.P. Beschler, Physical properties of sol-gel coatings, *J. Sol-Gel Sci. Technol.* 19 (2000) 23–29.

- [18] M. Pagliaro, R. Ciriminna, G. Palmisano, Silica-based hybrid coatings, *J. Mater. Chem.* 19 (2009) 3116–3126.
- [19] R.B.R. Garcia, F.S. da Silva, E.Y. Kawachi, New sol–gel route for $\text{SiO}_2/\text{ZrO}_2$ film preparation, *Colloids Surf. A Physicochem. Eng. Asp.* 436 (2013) 484–488.
- [20] I. Das, G. De, Zirconia based superhydrophobic coatings on cotton fabrics exhibiting excellent durability for versatile use, *Sci. Rep.* 5 (2015) 18501–18511, 18503.
- [21] B. Masheder, C. Urata, A. Hozumi, Transparent and hard zirconia-based hybrid coatings with excellent dynamic/thermo-responsive oleophobicity, thermal durability, and hydrolytic stability, *ACS Appl. Mater. Interfaces* 5 (2013) 7899–7905.
- [22] P. Rodič, J. Iskra, I. Milošev, A hybrid organic–inorganic sol–gel coating for protecting aluminium alloy 7075–T6 against corrosion in Harrison's solution, *J. Sol-Gel Sci. Technol.* 70 (2014) 90–103.
- [23] M. Catauro, F. Bollino, F. Papale, Preparation, characterization, and biological properties of organic–inorganic nanocomposite coatings on titanium substrates prepared by sol–gel, *J. Biomed. Mater. Res. A* 102 (2014) 392–399.
- [24] M.E.L. Wouters, D.P. Wolfs, M.C. van der Linde, J.H.P. Hovens, A.H.A. Tinnemans, Transparent UV curable antistatic hybrid coatings on polycarbonate prepared by the sol–gel method, *Prog. Org. Coat.* 51 (2004) 312–319.
- [25] W.L. Storm, J. Youn, K.P. Reighard, B.V. Worley, H.M. Lodaya, J.H. Shin, M.H. Schoenfish, Superhydrophobic nitric oxide-releasing xerogels, *Acta Biomater.* 10 (2014) 3442–3448.
- [26] Y. Huang, S. Yi, Z. Lv, C. Huang, Facile fabrication of superhydrophobic coatings based on two silica sols, *Colloid Polym. Sci.* 294 (2016) 1503–1509.
- [27] V. Oldani, G. Sergi, C. Pirola, C.L. Bianchi, Use of a sol-gel hybrid coating composed by a fluoropolymer and silica for the mitigation of mineral fouling in heat exchangers, *Appl. Therm. Eng.* 106 (2016) 427–431.
- [28] V. Oldani, R. del Negro, C.L. Bianchi, R. Suriano, S. Turri, C. Pirola, B. Sacchi, Surface properties and anti-fouling assessment of coatings obtained from perfluoropolyethers and ceramic oxides nanopowders deposited on stainless steel, *J. Fluor. Chem.* 180 (2015) 7–14.
- [29] A.R. Jennings, S.T. Iacono, Progress in fluorinated organically modified silicas, *Polym. Int.* 65 (2016) 6–10.
- [30] F. Boschet, B. Ameduri, (Co)polymers of chlorotrifluoroethylene: synthesis, properties, and applications, *Chem. Rev.* 114 (2014) 927–980.
- [31] F. Piccinini, M. Levi, S. Turri, Photoactive sol–gel hybrid coatings from modified fluoro-carbon polymers and amorphous titania, *Prog. Org. Coat.* 76 (2013) 1265–1272.
- [32] R. Suriano, V. Oldani, C.L. Bianchi, S. Turri, AFM nanomechanical properties and durability of new hybrid fluorinated sol-gel coatings, *Surf. Coat. Technol.* 264 (2015) 87–96.
- [33] Asahi Glass Company, Introduction, http://www.lumiflon.com/what_us/intro.html accessed in: 2016.
- [34] Y. Castro, M. Aparicio, R. Moreno, A. Durán, Silica-zirconia sol–gel coatings obtained by different synthesis routes, *J. Sol-Gel Sci. Technol.* 35 (2005) 41–50.
- [35] S. Graça, R. Colaço, R. Vilar, Micro-to-nano indentation and scratch hardness in the Ni–Co system: depth dependence and implications for tribological behavior, *Tribol. Lett.* 31 (2008) 177–185.
- [36] H. Hertz, Ueber die Berührung fester elastischer Körper, *J. Reine Angew. Math.* 1882 (1882) 156–171.
- [37] I.N. Sneddon, The relation between load and penetration in the axisymmetric Boussinesq problem for a punch of arbitrary profile, *Int. J. Eng. Sci.* 3 (1965) 47–57.
- [38] R. Suriano, C. Credi, M. Levi, S. Turri, AFM nanoscale indentation in air of polymeric and hybrid materials with highly different stiffness, *Appl. Surf. Sci.* 311 (2014) 558–566.
- [39] J.E. Sader, J.W.M. Chon, P. Mulvaney, Calibration of rectangular atomic force micro-scope cantilevers, *Rev. Sci. Instrum.* 70 (1999) 3967–3969.
- [40] J.E. Sader, J.A. Sanelli, B.D. Adamson, J.P. Monty, X. Wei, S.A. Crawford, J.R. Friend, I. Marusic, P. Mulvaney, E.J. Bieske, Spring constant calibration of atomic force micro-scope cantilevers of arbitrary shape, *Rev. Sci. Instrum.* 83 (2012) 103705.
- [41] J. Malzbender, G. de With, Scratch testing of hybrid coatings on float glass, *Surf. Coat. Technol.* 135 (2001) 202–207.
- [42] C.J. Fu, Z.W. Zhan, M. Yu, S.M. Li, J.H. Liu, L. Dong, Influence of Zr/Si molar ratio on structure, morphology and corrosion resistance of organosilane coatings doped with zirconium(IV) n-propoxide, *Int. J. Electrochem. Sci.* 9 (2014) 2603–2619.
- [43] L.Y.L. Wu, E. Chwa, Z. Chen, X.T. Zeng, A study towards improving mechanical properties of sol–gel coatings for polycarbonate, *Thin Solid Films* 516 (2008) 1056–1062.
- [44] M.L. González-Martín, L. Labajos-Broncano, B. Jańczuk, J.M. Bruque, Wettability and surface free energy of zirconia ceramics and their constituents, *J. Mater. Sci.* 34 (1999) 5923–5926.
- [45] R. Wagner, R. Moon, J. Pratt, G. Shaw, A. Raman, Uncertainty quantification in nano-mechanical measurements using the atomic force microscope, *Nanotechnology* 22 (2011) 455703.
- [46] B.A. Latella, M.V. Swain, M. Ignat, Indentation and fracture of hybrid sol-gel silica films, in: J. Nemecek (Ed.), *Nanoindentation in Materials Science*, InTech, 2012.
- [47] B.N. Zand, M. Mahdavian, Corrosion and adhesion study of polyurethane coating on silane pretreated aluminum, *Surf. Coat. Technol.* 203 (2009) 1677–1681.
- [48] G. Schottner, Hybrid sol-gel-derived polymers: applications of multifunctional materials, *Chem. Mater.* 13 (2001) 3422–3435.
- [49] C. Wilhelm, J.-L. Gardette, Infrared analysis of the photochemical behaviour of segmented polyurethanes: aliphatic poly(ether-urethane)s, *Polymer* 39 (1998) 5973–5980.
- [50] B. Ranby, J.F. Rabek, Photodegradation, Photo-oxidation and Photo-stabilization of Polymers, Wiley, London, 1975.
- [51] W. Schnabel, J. Kiwi, Photodegradation, in: H.H.G. Jellinek (Ed.), *Aspects of Degradation and Stabilization of Polymers*, Elsevier, Amsterdam 1978, pp. 195–246.